Article

SOURCE DATA   TRANSPARENT PROCESS

EMBO *reports*

β-Catenin-RAS interaction serves as a molecular switch for RAS degradation via GSK3β

Sang-Kyu Lee[1,2,†], Woo-Jeong Jeong[1,2,†], Yong-Hee Cho[1,2], Pu-Hyeon Cha[1,2], Jeong-Su Yoon[1,2], Eun Ji Ro[1,2], Sooho Choi[1,3], Jeong-Min Oh[1,3], Yunseok Heo[1,3], Hyuntae Kim[1,2], Do Sik Min[1,4], Gyoonhee Han[1,2], Weontae Lee[1,3] & Kang-Yell Choi[1,2,*] (ID)

Abstract

RAS proteins play critical roles in various cellular processes, including growth and transformation. RAS proteins are subjected to protein stability regulation via the Wnt/β-catenin pathway, and glycogen synthase kinase 3 beta (GSK3β) is a key player for the phosphorylation-dependent RAS degradation through proteasomes. GSK3β-mediated RAS degradation does not occur in cells that express a nondegradable mutant (MT) β-catenin. Here, we show that β-catenin directly interacts with RAS at the α-interface region that contains the GSK3β phosphorylation sites, threonine 144 and threonine 148 residues. Exposure of these sites by prior β-catenin degradation is required for RAS degradation. The introduction of a peptide that blocks the β-catenin-RAS interaction by binding to β-catenin rescues the GSK3β-mediated RAS degradation in colorectal cancer (CRC) cells that express MT β-catenin. The coregulation of β-catenin and RAS stabilities by the modulation of their interaction provides a mechanism for Wnt/β-catenin and RAS-ERK pathway cross-talk and the synergistic transformation of CRC by both *APC* and *KRAS* mutations.

Introduction

Adenomatous polyposis coli (*APC*) and *KRAS* mutations, which occur in 90% [1,2] and 40–50% [3,4] of human colorectal cancers (CRCs), respectively, are known to cooperate to synergistically promote CRC [5–7]. Although evidence of the cross-talk between Wnt/β-catenin signaling and the RAS/extracellular signal-regulated kinase (ERK) pathway is rapidly emerging, the molecular details that underlie this cross-talk are poorly understood [8].

The RAS/ERK pathway is regulated by Wnt/β-catenin signaling, and stability regulation of RAS is one of the key events for signaling cross-talk [9–11]. RAS proteins are subjected to glycogen synthase kinase 3 beta (GSK3β)-mediated polyubiquitination-dependent proteasomal degradation; GSK3β, the key component of the β-catenin destruction complex, phosphorylates RAS at the threonine (Thr) 144 and Thr-148 residues that are conserved among the RAS isoforms, which leads to the recruitment of the β-TrCP E3 linker [12,13]. Costabilization of β-catenin and RAS, particularly the KRAS mutant form, by *APC* mutations synergistically enhances the growth of CRC, and elevated levels of β-catenin and RAS are observed in CRC patient tissues, which indicates their pathological significance [12,14].

We have recently identified and characterized small molecules that suppress CRC cells via degradations of both β-catenin and RAS through inhibition of the Wnt/β-catenin pathway [15,16]. KYA1797K, one of the small molecules that functions via GSK3β activation by binding to the RGS domain of axin, inhibits the transformation of various CRC cells, including those that harbor *APC* and *KRAS* mutations [16]. Interestingly, KYA1797K does not induce the degradation of RAS and marginally inhibits the growth of CRC cells that express a nondegradable mutant (MT) β-catenin [16]. These results correlate with the results that RAS degradation by controlling Wnt/β-catenin signaling does not occur in cells that express MT β-catenin [11].

These observations have enabled us to investigate a molecular mechanism for the β-catenin-dependent RAS stability regulation. Here, we show that β-catenin directly interacts with RAS at the α-interface region that contains the GSK3β phosphorylation sites involved in the degradation of RAS, as illustrated by structural analyses using nuclear magnetic resonance (NMR) spectroscopy. The prior β-catenin degradation exposes the Thr-144 and Thr-148 residues, thereby enabling phosphorylation by GSK3β and the

---

1   Translational Research Center for Protein Function Control, Yonsei University, Seoul, Korea
2   Department of Biotechnology, College of Life Science and Biotechnology, Yonsei University, Seoul, Korea
3   Department of Biochemistry, College of Life Science and Biotechnology, Yonsei University, Seoul, Korea
4   Department of Molecular Biology, College of Natural Science, Pusan National University, Pusan, Korea
    *Corresponding author. Tel: +82 2 2123 6589; E-mail: kychoi@yonsei.ac.kr
    †These authors contributed equally to this work

subsequent proteasomal degradation of RAS. The importance of the release of RAS from MT β-catenin for its degradation and its role in the suppression of cellular transformation by *KRAS* mutations were validated using a competitor peptide that blocked the β-catenin-RAS interaction. We have also confirmed the importance of the sequential degradations of β-catenin and RAS in the suppression of CRC in a mouse xenograft model. Overall, in a resting state, RAS proteins are subjected to degradation by GSK3β; however, the costabilization of both β-catenin and RAS by GSK3β inactivation, induced by *APC* loss, provides a mechanical basis of the synergistic transformation by both *APC* and *KRAS* mutations in CRC. A stepwise degradation of β-catenin and RAS, particularly mutant KRAS, may be a potential strategy for controlling CRC by targeting the Wnt/β-catenin pathway.

Results

RAS degradation via the Wnt/β-catenin pathway requires prior β-catenin degradation

RAS degradation by controlling Wnt/β-catenin signaling does not occur in cells that express a nondegradable mutant (MT) β-catenin [11,16]; thus, we investigated the effects of axin, a negative regulator of Wnt/β-catenin signaling, on the stability of both β-catenin and RAS in several cell lines with different mutational statuses of *CTNNB1* (encoding β-catenin). We interestingly observed that the levels of both β-catenin and RAS were reduced together with RAS downstream ERK activities by the overexpression of axin in DLD1 and wild-type (WT) HCT116 CRC cells harboring WT *CTNNB1*; however, these reductions were not observed in MT HCT116, SW48 CRC cells, and HepG2 hepatocarcinoma cells harboring MT *CTNNB1* (Fig 1A). Furthermore, the depletion of MT β-catenin using two independent siRNA-mediated knock-downs in MT HCT116 cells significantly induced RAS destabilization in a polyubiquitination-dependent manner (Fig 1B and C). The reductions in both β-catenin and RAS were confirmed by immunocytochemical analyses (Fig EV1A).

Because the degradations of both β-catenin and RAS occur via GSK3β-mediated phosphorylation [12,17], we further assessed the effects of GSK3β overexpression on RAS degradation in HEK293 cells that expressed WT or MT β-catenin. GSK3β overexpression reduced both the β-catenin and RAS levels along with increases in their phosphorylation at Ser-33/Ser-37 and Thr-144/Thr-148, respectively, in HEK293 cells that expressed WT β-catenin, but not in cells that expressed MT β-catenin (Fig 1D). In addition, the phosphorylation of both β-catenin and RAS was decreased together with increments of their protein levels in HEK293 cells treated with Wnt3a; however, these effects were mostly inhibited by β-catenin knockdown (Fig 1E).

We previously identified KYA1797K, a small molecule that simultaneously destabilizes both β-catenin and RAS via the activation of GSK3β by binding to the RGS domain of axin [16]. In addition, tankyrase inhibitors, such as XAV939, which degrade β-catenin through axin stabilization, also destabilize both β-catenin and RAS, although they have a different mode of action from KYA1797K [16]. Therefore, we tested the requirement of WT *CTNNB1* for RAS degradation induced by KYA1797K or XAV939 in HCT116 isogenic CRC cells that harbored WT or MT *CTNNB1*. KYA1797K or XAV939

effectively degraded both β-catenin and RAS in WT HCT116 cells; however, these reductions did not occur in MT HCT116 cells (Fig 1F). This finding was further confirmed by the absence of RAS degradation in KYA1797K- or XAV939-treated HEK293 and DLD1 cells that overexpressed MT β-catenin (Fig EV1B). In addition, the levels of both β-catenin and RAS were time-dependently reduced by KYA1797K in cells that expressed WT β-catenin with the approximate $t_{1/2}$ values of 3 h and 6 h of β-catenin and RAS, respectively (Fig EV1C).

The requirement of WT β-catenin for RAS degradation in a polyubiquitination-dependent manner by KYA1797K was confirmed as shown by immunocytochemical and polyubiquitination analyses (Fig 1G and H). Furthermore, the growth of WT HCT116 and MT HCT116 cells was reduced by 90 and 10%, respectively, by KYA1797K treatment (Fig 1I). The differential effects of KYA1797K on growth depend on the mutation status of *CTNNB1* and are correlated with the effects on RAS stability. Similarly, the growth of *CTNNB1*-mutated HCT116 and SW48 cells was marginally reduced by KYA1797K; however, the pan-RAS levels and ERK activities were not reduced (Fig EV1D and E). This marginal growth inhibition by KAY1797K in *CTNNB1*-mutated cells, which occur independently of β-catenin and RAS destabilizations, was also observed in a previous study [16]. Overall, GSK3β-mediated RAS degradation by negative Wnt/β-catenin signaling required prior β-catenin degradation.

C-terminal domain of β-catenin directly interacts with RAS at a region that contains the GSK3β phosphorylation sites

We subsequently determined whether RAS and β-catenin interacted with each other because prior β-catenin degradation is required for RAS phosphorylation and both proteins are phosphorylated by GSK3β. Endogenous β-catenin and pan-RAS were coimmunoprecipitated in the whole cell extracts of HEK293 cells (Fig EV2A) and DLD1 cells (Fig 2A). The β-catenin-RAS interaction was dependent on Wnt/β-catenin signaling as shown by the increment of the β-catenin-RAS interaction in HEK293 cells treated with Wnt3a-CM (Fig 2B). The β-catenin-RAS interaction was further confirmed by the specific pull-down of GFP-β-catenin with glutathione S-transferase (GST)-HRAS, but not GFP-Mock (Fig EV2B). To better understand the β-catenin-RAS interaction, we separated the cytosol and nucleus portions of MT HCT116 extracts. Although MT β-catenin was localized at both the cytosol and nucleus portions, RAS was mainly presented at the cytosolic portion (Fig 2C). Moreover, the β-catenin-RAS interaction was mostly observed in the cytosolic fraction, but not the nuclear fraction, of the HCT116 cell extracts (Fig 2C). The specification of the β-catenin-RAS interaction at the cytosol was further confirmed by the enhancement of their interaction as shown using an *in situ* proximity ligation assay (Fig 2D). These results were also supported by the higher cytosolic β-catenin-RAS interaction in MT HCT116 cells than in WT HCT116 cells (Fig EV2C).

To determine the binding motif between β-catenin and RAS, we designed and constructed deletion mutants of β-catenin and RAS, respectively. Considering the GSK3β phosphorylation sites involving the degradation of RAS [12,16], we designed the deletion mutant without the Thr-144 and Thr-148 residues (Δ131–165). A GST-fused full-length (FL) HRAS and a MT HRAS that lacked the C-terminal hypervariable regions (HVRs) were both pulled down by the His-tagged β-catenin (His-β-catenin) (Fig 2E). Interestingly, the HRAS
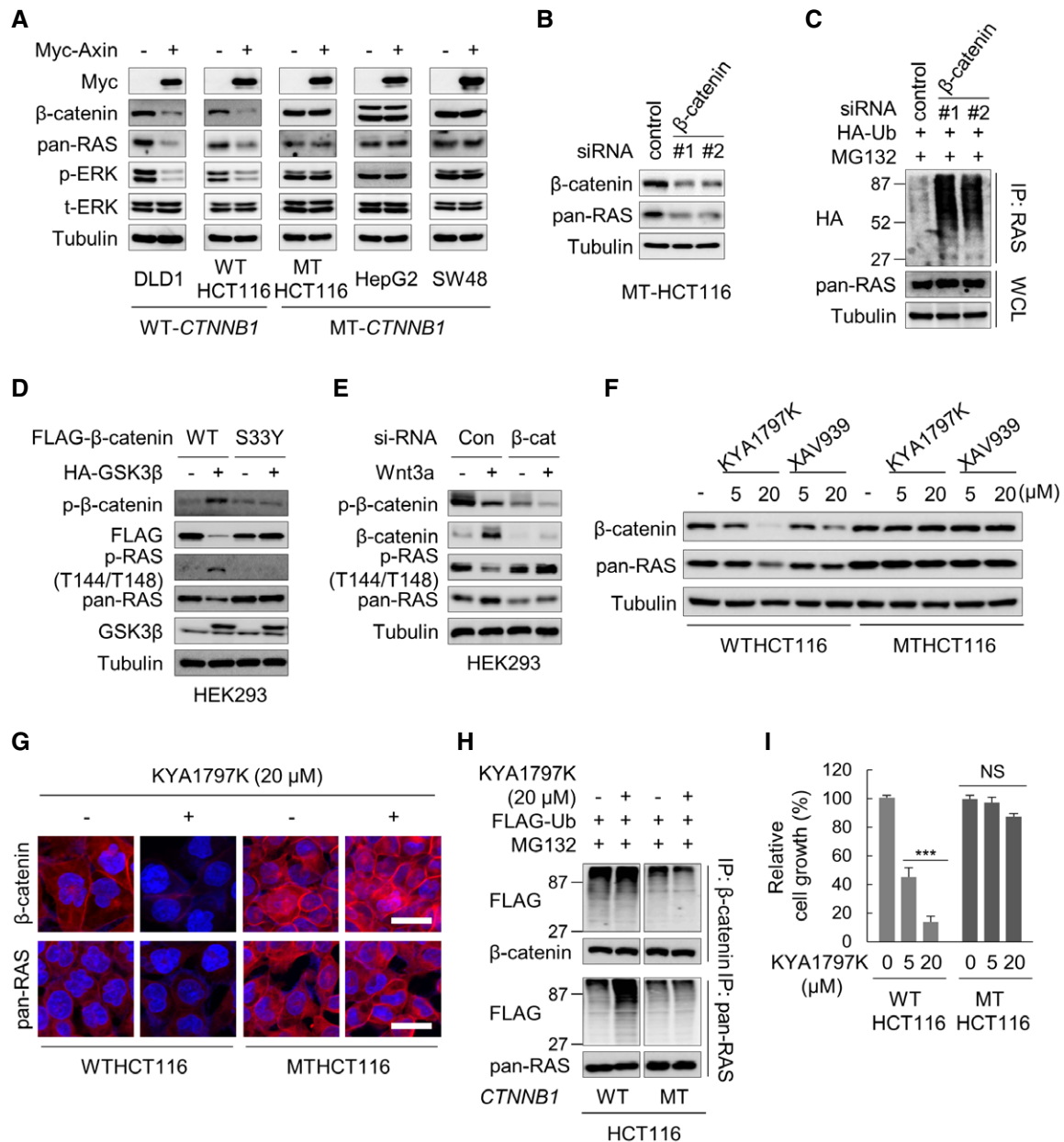
Figure 1.   Prior β-catenin degradation is required for RAS degradation via the Wnt/β-catenin pathway.

A   Immunoblot (IB) analyses of the levels of β-catenin and RAS in DLD1, WT HCT116, MT HCT116, HepG2, and SW48 cells transfected with Myc-axin for 36 h.

B   Effects of β-catenin knock-down on polyubiquitination-dependent degradation of RAS. IB analyses of MT HCT116 cells transfected with control or two independent β-catenin siRNAs for 48 h.

C   Polyubiquitination assays of MT HCT116 cells cotransfected with two independent β-catenin siRNAs and HA-ubiquitin (Ub) for 72 h in the presence of the proteasomal inhibitor MG132, and WCLs were immunoprecipitated with an anti-pan-RAS antibody.

D   IB analyses of HEK293 cells transfected with WT- or S33Y-Flag-β-catenin with or without HA-GSK3β for 36 h.

E   IB analyses of HEK293 cells transfected with β-catenin siRNA or control siRNA for 48 h and then treated with L-cell-conditioned medium (L-CM) or Wnt3a-CM for 8 h.

F   Effects of KYA1797K or XAV939 on degradation of β-catenin and RAS in isogenic HCT116 cells harboring WT or MT *CTNNB1*. IB analyses of β-catenin and RAS levels in WT or MT HCT116 cells treated with 5 or 20 μM of KYA1797K or XAV939 for 24 h.

G   ICC analyses of WT or MT HCT116 cells treated with 20 μM of KYA1797K for 24 h. Scale bars, 10 μm.

H   For polyubiquitination assays, WT or MT HCT116 cells were transfected with FLAG-Ub for 24 h and then treated with 20 μM of KYA1797K for 24 h in the presence of MG132. WCLs were immunoprecipitated with β-catenin or pan-RAS antibody and subjected to IB analyses to detect each protein.

I   The 3-(4,5-dimethylthiazol-2yl)-2-5-diphenyltetrazolium bromide (MTT) assays were performed for measurements of growth of WT or MT HCT116 cells treated with the indicated concentrations of KYA1797K. Data are represented as the mean ± SD ($n = 3$). Statistical significances were assessed using two-sided Student's *t*-tests, ***$P < 0.001$. NS, not significant.
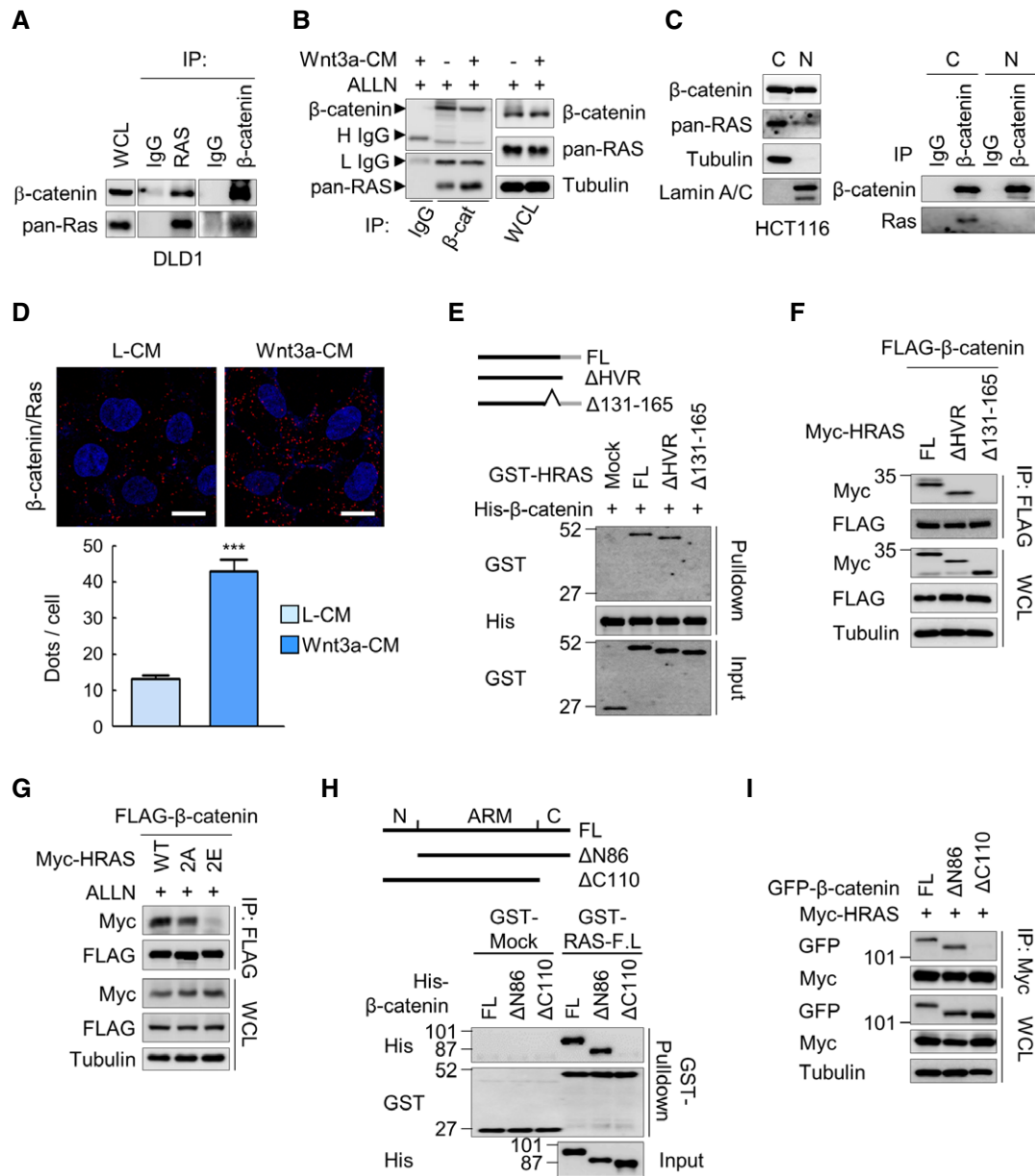
Source data are available online for this figure.

Figure 2. β-Catenin directly interacts with RAS at a region that contains GSK3β phosphorylation sites.

A   Analyses of the interaction between β-catenin and RAS. WCLs of DLD1 cells were immunoprecipitated with β-catenin or pan-RAS antibody and subjected to IB analyses.

B   IB analyses of indicated proteins in the samples immunoprecipitated with anti-β-catenin antibody with WCLs of HEK293 cells treated with Wnt3a-CM.

C   Left panel: MT HCT116 cell extracts were fractionated as cytosolic and nuclear portions and subjected to IB analyses, respectively. Right panel: The cytosolic and nuclear fractions were immunoprecipitated with anti-β-catenin antibody and subjected to IB analyses.

D   β-Catenin-RAS interaction was visualized by *in situ* proximity ligation assay in HEK293 cells treated with L-CM or Wnt3a-CM. Scale bars, 20 μm. The proximity ligation signal was quantified in 10 randomly distributed microscopic images that contained > 100 cells. Data are represented as the mean ± SD (n = 3). Statistical significances were assessed using two-sided Student's *t*-tests, ***P < 0.001.

E   *In vitro* pull-down analyses to identify β-catenin binding region of RAS. Upper panel: Schematic of the HRAS full-length (FL) or two deletion mutants. Lower panel: Purified GST-HRAS-FL, GST-HRAS-ΔHVR, or GST-HRAS-Δ131–165 proteins were pulled down with purified His-β-catenin-FL protein and subjected to IB analyses.

F   IB analyses of IP with FLAG antibody in WCLs of HEK293 cells cotransfected with FLAG-β-catenin and Myc-HRAS-FL, Myc-HRAS-ΔHVR, or Myc-HRAS-Δ131–165 for 32 h.

G   IB analyses of IP with FLAG antibody in WCLs of HEK293 cells cotransfected with FLAG-β-catenin and Myc-HRAS-WT, Myc-HRAS-2A, or Myc-HRAS-2E for 32 h.

H   Upper panel: Schematic of the β-catenin-FL or two deletion mutants. Lower panel: Purified His-β-catenin-FL, His-β-catenin-ΔN86, or His-β-catenin-ΔC110 proteins were pulled down with purified GST-HRAS-FL protein and subjected to IB analyses.

I   IB analyses of IP with Myc antibody with WCLs of HEK293 cells cotransfected with Myc-HRAS and GFP-β-catenin-FL, GFP-β-catenin-ΔN86, or GFP-β-catenin-ΔC110 for 32 h.

Source data are available online for this figure.

amino acids 131–165 were required for the β-catenin interaction as indicated by the absence of pull-down of the GST-HRAS MT that lacked the region (HRAS-Δ131–165) by His-β-catenin (Fig 2E). This finding was further confirmed by the absence of immunoprecipitation (IP) of Myc-HRAS-Δ131–165 by FLAG-β-catenin (Fig 2F), which indicates that the region containing the GSK3β phosphorylation sites of RAS is required for β-catenin interaction. Therefore, we determined the roles of the threonine residues of RAS in β-catenin binding using phospho-defective (T144/T148A, 2A) and phospho-mimetic (T144/148E, 2E) mutants [12]. β-Catenin specifically interacted with nonphosphorylated RAS as shown by its co-IP with HRAS-2A, but not with HRAS-2E (Fig 2G). To further confirm the importance of the status of RAS phosphorylation at Thr-144 and Thr-148 for the binding of β-catenin, we detected phosphorylated RAS in the β-catenin-RAS complex using phospho-specific anti-RAS antibody. Phosphorylated RAS was not detected, although a substantial amount of RAS was detected in the β-catenin immune complex (Fig EV2D). These results suggest that the status of RAS phosphorylation at Thr-144 and Thr-148 is important for the β-catenin-RAS interaction. β-Catenin interacted with all major isotypes of RAS (N, K, and HRAS), which have conserved amino acid sequences, including the phosphorylation sites, and vary only in their HVRs (Fig EV2E).

The β-catenin mutant that lacked the C-terminal region (ΔC110), which included the transactivation domain that forms a complex with transcriptional regulators such as CREB-binding protein (CBP) or inhibitors of β-catenin and Tcf (ICAT), did not bind to RAS as shown by the GST-pull-down or co-IP assays. However, the FL and N-terminal deletion mutant (ΔN86) of β-catenin interacted with RAS (Fig 2H and I). Together, the C-terminal domain of β-catenin directly interacts with RAS at a region that contains the GSK3β phosphorylation sites.

β-Catenin interacts with and masks RAS at the α-interface that contains the GSK3β phosphorylation sites

To determine the binding affinity between β-catenin and RAS, we performed a fluorescence spectroscopy analysis using the purified recombinant proteins, β-catenin and KRAS. The dissociation constants (K_d) of intact β-catenin for KRAS were evaluated as 1.19×10^{-4} M (Fig 3A). To further characterize the interaction between β-catenin and KRAS, we analyzed the chemical shift perturbations by NMR spectra using a β-catenin C-terminal fragment that contained residues 661–781 and intact KRAS. We observed the peak shifts of KRAS following β-catenin binding and could present the chemical shift perturbation by quantifying the chemical shift of each residue of KRAS (Appendix Fig S1). When titrated with the β-catenin fragment, the L19, I46, I142, E162, R164, and K165 residues of KRAS appeared as amino acid residues showed chemical shift changes > 0.02 (Fig 3B and Appendix Fig S1) and indicated as the potential β-catenin binding residues. These residues are mostly localized at the α-interface [18], which is mainly orientated parallel to the membrane and is composed of residues T127-K167 (α4, β6, and α5), the N-terminus of β1, and a loop between β2 and β3 (Fig 3C and D, and Appendix Fig S1B). The Thr-144 and Thr-148 residues, the GSK3β phosphorylation sites required for its degradation, are localized at the α-interface region, particularly near I142 and L19 (Fig 3C). Although β-catenin structure is not fully

determined, we illustrated a ribbon diagram for the predicted interface between β-catenin and RAS, representing that the α-interface of KRAS provides a large accessible surface area to potentially interact with the β-catenin C-terminal domain in the dynamic state (Fig 3E). Together, β-catenin directly interacted with and masked RAS at the α-interface that contained the GSK3β phosphorylation sites.

Prior β-catenin degradation exposes the GSK3β phosphorylation sites of RAS required for its subsequent degradation

Because the mechanism of RAS destabilization was dependent on the β-catenin status, we investigated whether prior phosphorylation and degradation of β-catenin were required for subsequent RAS degradation. β-Catenin phosphorylation at Ser-33 and Ser-37 was induced in WT HCT116 cells; however, it did not occur in MT HCT116 cells (Fig 4A). The increment of the GSK3β binding affinity and subsequent phosphorylation of RAS at Thr-144 and Thr-148 by KYA1797K occurred in the WT HCT116 cells and did not occur in the MT HCT116 cells (Fig 4A). Consequently, the β-catenin-RAS interaction was reduced by KYA1797K in WT HCT116 cells, but not in MT HCT116 cells (Fig 4A). As the KYA1797K treatment effects, GSK3β overexpression reduced the levels of both β-catenin and RAS along with increments of their phosphorylation in HEK293 cells that expressed WT β-catenin, but not in cells that expressed MT β-catenin (Fig 1D). Furthermore, the affinity of the β-catenin-RAS interaction was decreased by the overexpression of catalytically active mutant (GSK3β-CA) that induced GSK3β binding and β-catenin and RAS phosphorylation, but not by catalytically inactive mutant (GSK3β-KD) (Fig EV3A).

The Wnt/β-catenin signal-dependent stabilization of RAS, which was attributed to the masking of the phosphorylation sites of RAS by binding stabilized β-catenin, was confirmed by the enhancement of the β-catenin-RAS binding affinity by Wnt3a-CM treatment (Fig 4B). The phosphorylation levels of β-catenin and RAS were decreased, and their binding affinities to GSK3β, including the active form (pY216) and β-TrCP, were reduced in HEK293 cells treated with Wnt3a-CM (Fig 4B). In addition, the reduction in the β-catenin-RAS interaction by GSK3β-mediated β-catenin phosphorylation correlates with the observation that the blockade of the Wnt3a-induced β-catenin-RAS interaction by treatment of KYA1797K induces the phosphorylation of both β-catenin and RAS for their degradation (Fig EV3B). In contrast to RAS degradation, β-catenin was degraded by GSK3β overexpression or KYA1797K treatment even in DLD1 cells that expressed KRAS-2A, a nondegradable mutant KRAS that replaced threonine 144 and threonine 148 with alanine, respectively (Fig 4C). These results indicate that the phosphorylation and degradation of RAS were dispensable for β-catenin degradation. Together, prior phosphorylation and degradation of β-catenin are required for subsequent GSK3β-mediated RAS degradation.

Interference of the MT β-catenin-RAS interaction rescues RAS degradation

Because MT β-catenin prevented RAS degradation by masking its phosphorylation sites, we designed a β-catenin binding region of RAS (BBR) peptide, which contains RAS amino residues from 131 to 165, including the Thr-144 and Thr-148 phosphorylation sites, and hypothesized that BBR peptide, which blocks their interaction by
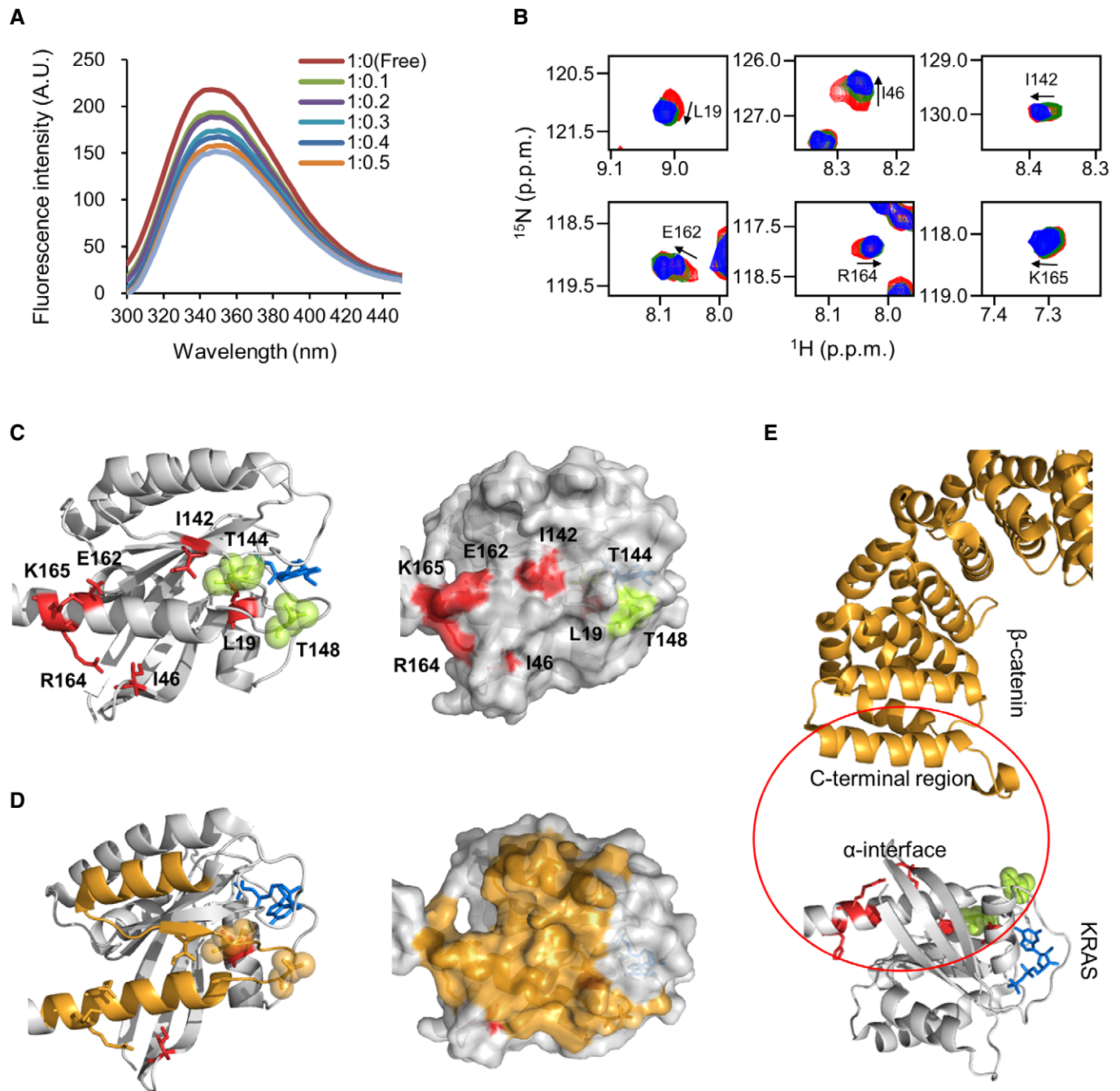
Figure 3. β-Catenin interacts with RAS at the α-interface that contains the GSK3β phosphorylation sites.

A   Fluorescence spectroscopy analyses of the interaction between β-catenin and KRAS using purified recombinant proteins, intact β-catenin and KRAS. Molar ratios of β-catenin and KRAS are presented. A.U., absorbance units.

B   Nuclear magnetic resonance (NMR) titration for ^{15}N-labeled KRAS (full-length, 1–188) with β-catenin (C-terminal fragment, 661–781). The titration points are indicated in red (1:0), green (1:5), and blue (1:10). A gradual perturbation in chemical shift is indicated by the arrow.

C, D   A molecular docking model for NMR spectra data represented by a ribbon diagram (left panels of C and D) and structure-based surface area (right panels of C and D) of KRAS (C; chemical shift residues, red; phosphorylation sites Thr-144/Thr-148, green; GTP/GDP loading site, blue). The α-interface area is presented as yellow (D).

E   The interface (red circle) for interaction between C-terminal domain of β-catenin (helix C) and α-interface of KRAS represented by a ribbon diagram.

competitive β-catenin binding, could rescue the GSK3β-mediated RAS degradation (Appendix Fig S2A). When overexpressed in HEK293 cells, the BBR peptide interacted with β-catenin as shown by *in vitro* pull-down (Fig 5A) and co-IP (Fig 5B) analyses. In addition, BBR overexpression significantly reduced the β-catenin-RAS interaction in HEK293 cells (Fig 5B).
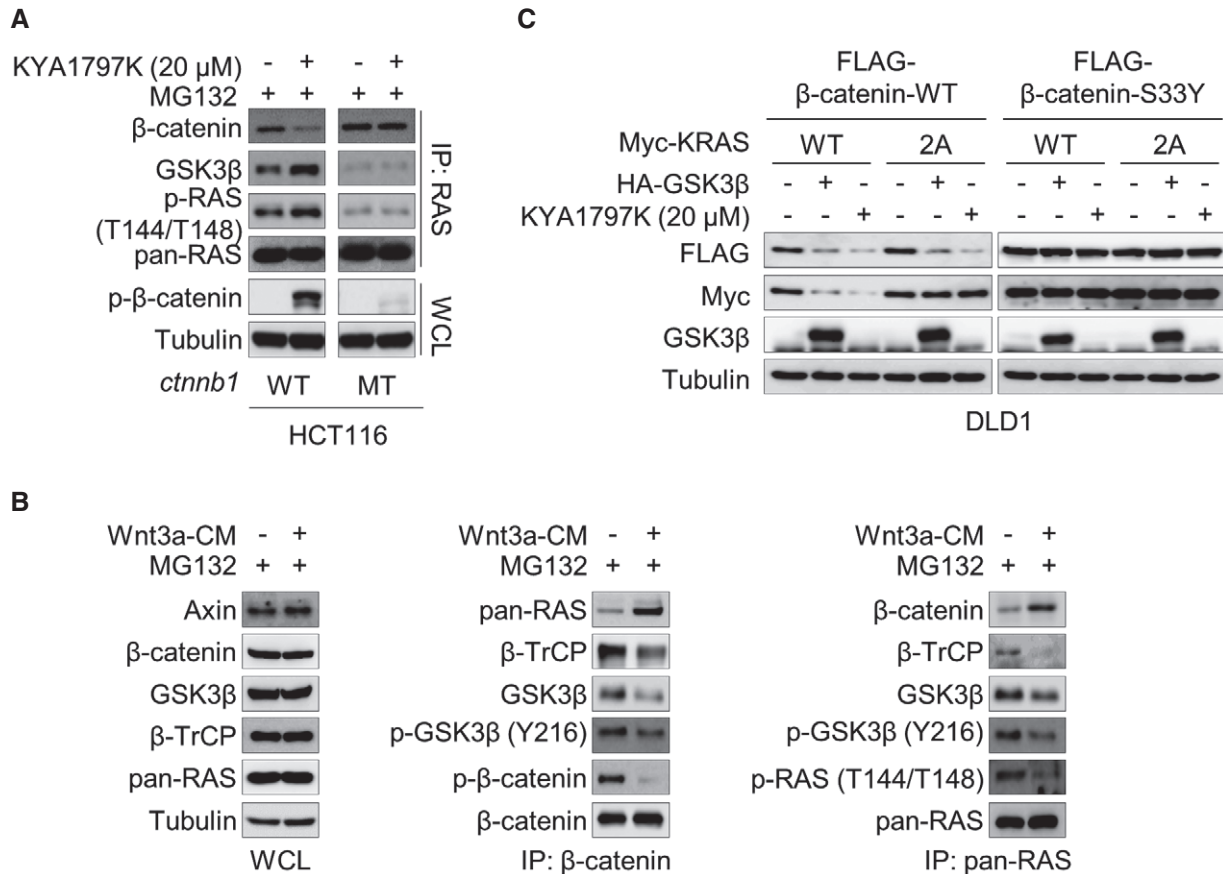
Figure 4. Prior β-catenin degradation is required for RAS degradation via a stepwise mechanism.

A   Effects of KYA1797K on the interaction and phosphorylation of β-catenin and pan-RAS. WT or MT HCT116 cells were treated with 20 μM of KYA1797K in the presence of MG132. WCLs were immunoprecipitated with pan-RAS antibody and subjected to IB analyses.

B   Effects of Wnt3a-CM treatment on the formation of β-catenin destruction complex and phosphorylation of β-catenin and RAS in HEK293 cells treated with L-CM or Wnt3a-CM in the presence of MG132 for 8 h. WCLs were immunoprecipitated with β-catenin or pan-RAS antibodies and subjected to IB analyses.

C   IB analyses were performed to detect β-catenin and pan-RAS in DLD1 cells cotransfected with FLAG-β-catenin-WT or FLAG-β-catenin-MT and Myc-KRAS-WT or Myc-KRAS-2A for 24 h and then treated or transfected with 20 μM of KYA1797K or HA-GSK3β for 24 h, respectively.

Source data are available online for this figure.

Although KYA1797K did not degrade both β-catenin and RAS in cells that expressed MT β-catenin, KYA1797K reduced the RAS levels without changing the β-catenin levels by overexpression of BBR in these cells (Fig 5C and Appendix Fig S2B). Similarly, XAV939 also induced RAS degradation in MT HCT116 cells that overexpressed BBR (Appendix Fig S2C). The levels of RAS were specifically reduced along with the increments of its phosphorylation and polyubiquitination by KYA1797K in MT HCT116 cells that overexpressed BBR (Fig 5D and E).

To confirm the importance of the regulation of RAS phosphorylation at Thr-144 and Thr-148 in β-catenin binding, we tested the effects of a mutant peptide in which the phosphorylation residues are replaced with the phospho-mimetic glutamic acid (BBR-2E). In contrast to BBR, BBR-2E overexpression did not change the β-catenin-RAS interaction (Fig 5F) and resulted in the absence of polyubiquitination and degradation of RAS by KYA1797K in MT HCT116 cells (Fig 5G and H). Similarly, the ineffectiveness of BBR-2E on the RAS degradation was confirmed by treatment of XAV939 (Appendix Fig S2D). Therefore, these data also supported a novel

two-step mechanism for the sequential degradations of β-catenin and RAS dependent on their phosphorylation.

A peptide-mediated interference of the β-catenin-RAS interaction sensitizes the anti-transformation effects of small molecular RAS destabilizers on CRC cells with *CTNNB1* mutations

To determine whether RAS degradation by blocking the β-catenin-RAS interaction is related to cellular function, we designed the protein transduction domain (PTD)-fused BBR peptide (PTD-BBR) conjugated with fluorescein isothiocyanate (FITC) and assessed the transduction ability of PTD-BBR as shown by flow cytometry and ICC analyses (Fig EV4A and B). Treatment of PTD-BBR induced RAS degradation and dose-dependent growth inhibition by KYA1797K in MT HCT116 and SW48 CRC cells with *CTNNB1* mutations (Fig 6A and B). Similarly, the overexpression of BBR peptide dose-dependently increased the effects of KYA1797K on the growth inhibition of MT HCT116 and SW48 cells (Fig EV4C). In addition, the cotreatment of PTD-BBR and KYA1797K induced apoptotic Sub-G0 phase and
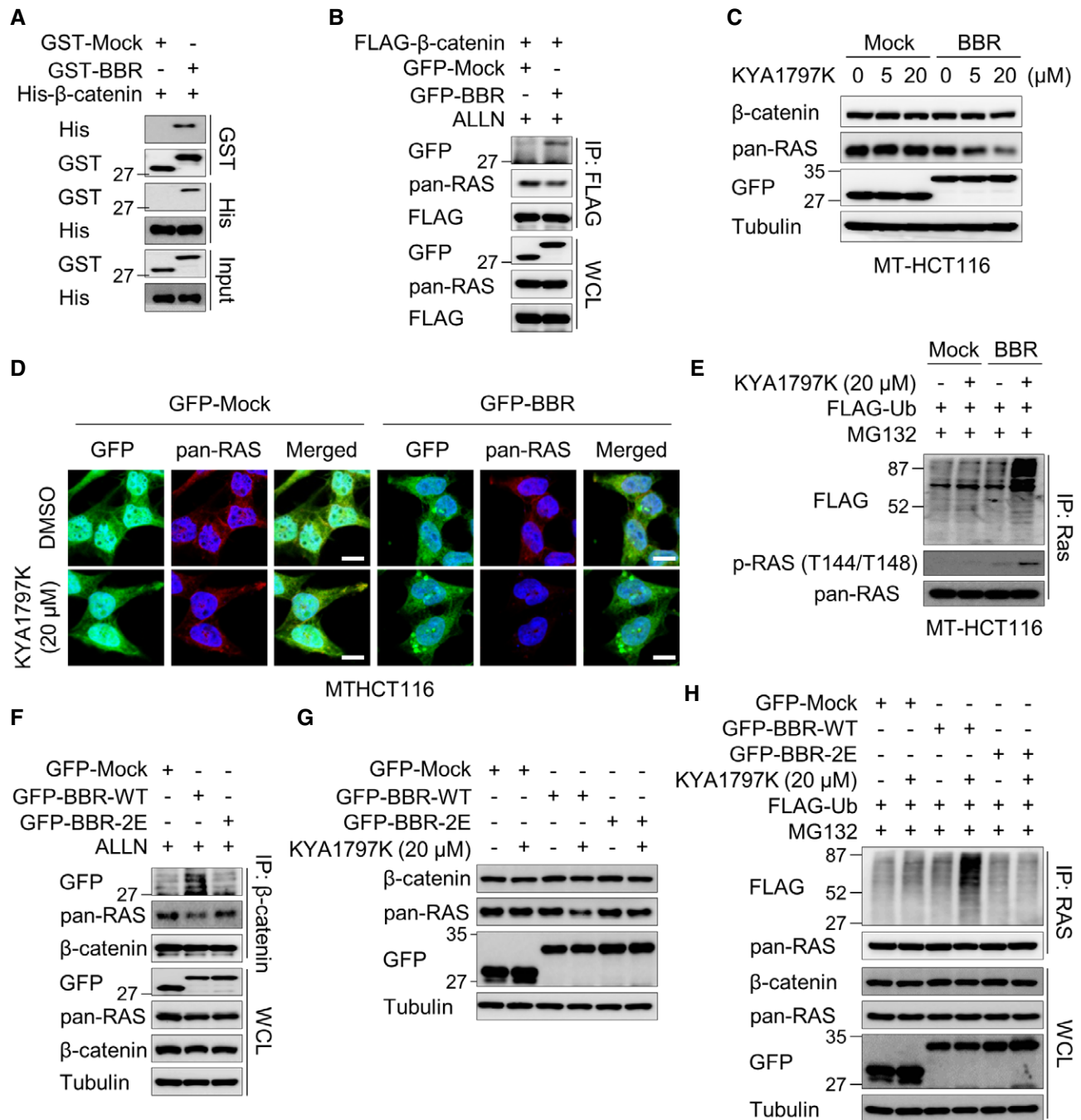
Figure 5. Blockage of β-catenin-RAS interaction via a competing peptide induces RAS degradation in *CTNNB1*-mutated CRC cells.

A   IB analyses to determine the interaction between β-catenin and BBR peptide by *in vitro* pull-down assays using purified His-β-catenin and GST-BBR proteins.

B   IB analyses of IP with FLAG antibody and WCLs from HEK293 cells cotransfected with FLAG-β-catenin and GFP-BBR or GFP-Mock in the presence of proteasome inhibitor, ALLN, for 24 h.

C, D   Effects of BBR overexpression on KYA1797K-induced RAS degradation. IB (C) and ICC (D; Scale bars, 10 μm) analyses to detect levels of RAS in MT HCT116 cells transfected with GFP-Mock or GFP-BBR for 24 h and then treated with 20 μM of KYA1797K for 24 h.

E   MT HCT116 cells were cotransfected with GFP-Mock or GFP-BBR and FLAG-Ub for 24 h and then treated with 20 μM of KYA1797K in the presence of MG132 for 8 h, and WCLs were immunoprecipitated with pan-RAS antibody.

F   IB analyses of IP with β-catenin antibody in MT HCT116 cells transfected with GFP-BBR-WT, GFP-BBR-2E, or GFP-Mock in the presence of ALLN for 24 h.

G   IB analyses of MT HCT116 cells transfected with GFP-Mock, GFP-BBR-WT, or GFP-BBR-2E for 24 h and then treated with 20 μM of KYA1797K for 24 h.

H   MT HCT116 cells were transfected with GFP-Mock, GFP-BBR-WT, or GFP-BBR-2E together with FLAG-Ub with or without 20 μM of KYA1797K for 24 h, and MG132 was treated for 8 h before harvesting cells. WCLs were immunoprecipitated with pan-RAS antibody and subjected to IB analyses.

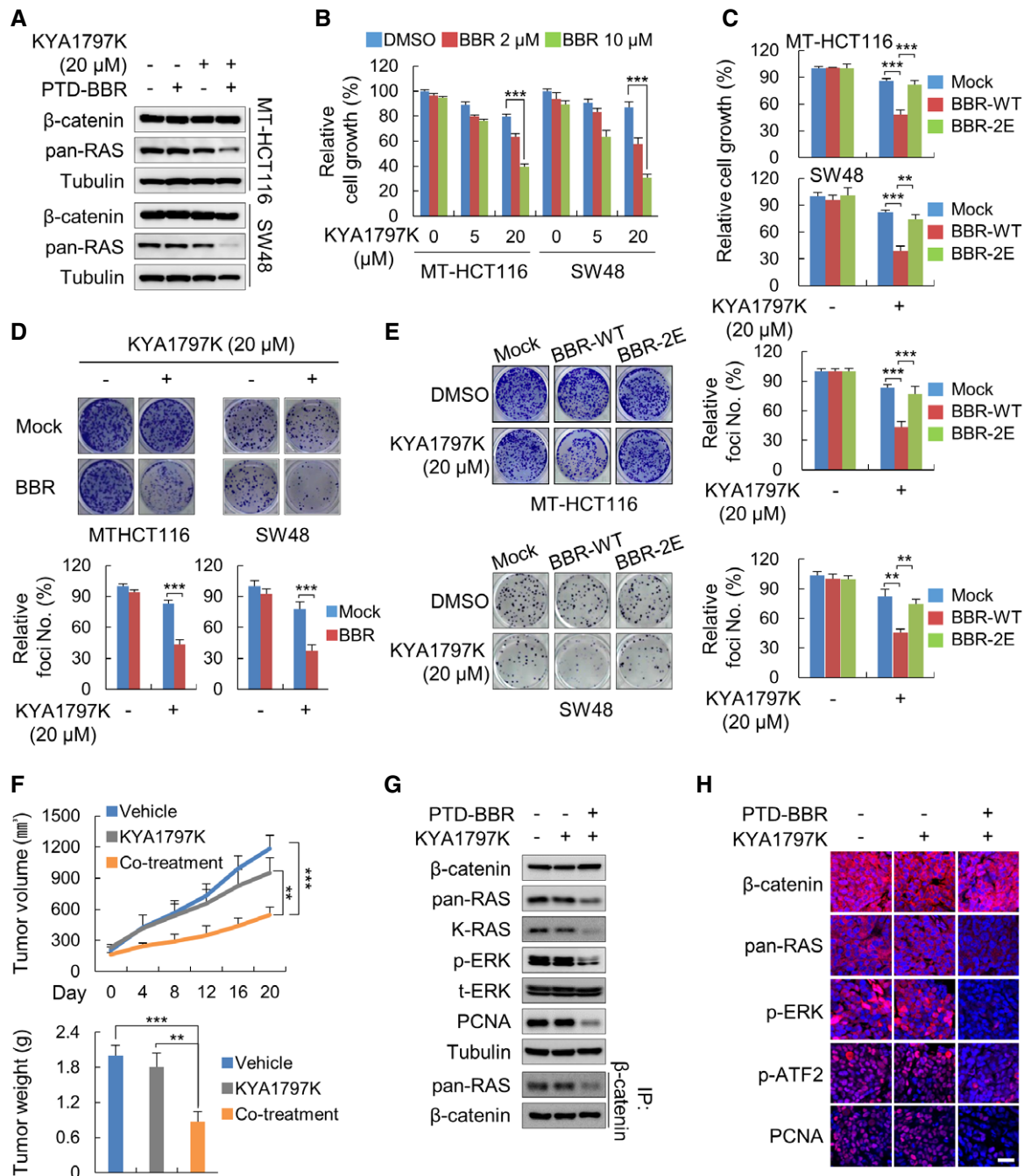Source data are available online for this figure.

Figure 6. Interference of the β-catenin-RAS interaction suppresses the synergistic transformation and tumor growth induced by *CTNNB1* and *KRAS* mutations via RAS degradation.

A, B   Effects of KYA1797K and PTD-BBR on RAS degradation and cell growth. IB (A) and MTT (B) assays of MT HCT116 or SW48 cells treated with indicated conditions for 24 and 96 h, respectively. Data are represented as the mean ± SD (n = 3).

C–E   Effects of overexpression of GFP-BBR-WT or GFP-BBR-2E mutant on KYA1797K-induced growth and transformation of CRC cells. MT HCT116 or SW48 cells were transfected with GFP-BBR-WT, GFP-BBR-2E, or GFP-Mock for 24 h and then treated with KYA1797K via indicated conditions. MTT (C) assays were performed for measurements of cell growth, and foci formation assays (D and E) were performed to detect cellular transformation. Data are represented as the mean ± SD (n = 3).

F   Effects of cotreatments with KYA1797K and PTD-BBR on xenografted tumor growth. MT HCT116 cells were subcutaneously injected in nude mice with subsequent i.p. injection of vehicle, 20 mg/kg of KYA1797K, or a cotreatment of PTD-BBR (25 mg/kg) and KYA1797K (20 mg/kg) for 20 days. Tumor volumes (upper panel) were measured every 4 days, and tumor weights (lower panel) were measured at the times of sacrifice. Data are represented as the mean ± SD (four mice per group).

G   WCLs prepared from tumor tissues were immunoprecipitated with anti-β-catenin antibody. WCLs or co-IP samples were subjected to IB analyses.

H   IHC analyses of tissue sections incubated with the indicated antibodies and then counterstained with DAPI. Scale bar, 20 μm.

Data information: Statistical significances were assessed by two-sided Student's *t*-tests, **$P < 0.01$ and ***$P < 0.001$.
Source data are available online for this figure.

Annexin V-positive cells without showing significant cell cycle arrest (Appendix Fig S3). These results suggest that the inhibition of cell growth by the cotreatment of PTD-BBR and KYA1797K is caused by the induction of apoptosis. In contrast to BBR, BBR-2E did not show an inhibitory effect on the growth of MT HCT116 and SW48 cells when treated with KYA1797K (Figs 6C and EV4D and E). The ineffectiveness of BBR-2E treatment on RAS degradation in MT HCT116 cells treated with KYA1797K was also confirmed by ICC (Fig EV4F). In addition, the ineffectiveness of BBR-2E on the KYA1797K-mediated anti-proliferation was further confirmed by BrdU incorporation assays (Fig EV4G). The cellular transformation monitored by anchorage-independent cell growth was inhibited by KYA1797K specifically in cells that overexpressed BBR peptide (Fig 6D), but not in cells that overexpressed BBR-2E peptide (Fig 6E). As with KYA1797K treatment, the specific effects of the BBR peptide on the growth and transformation of CRC cells with *CTNNB1* mutations were also observed in XAV939 treatment (Fig EV4H and I). Together, the effects of β-catenin-dependent stability regulation of RAS on the growth and transformation were confirmed.

To further investigate the *in vivo* effects of RAS degradation by blocking the β-catenin-RAS interaction on the growth of CRC, we used the PTD-BBR peptide. Mice bearing xenograft tumors generated by MT HCT116 cells were i.p. injected with PTD-BBR and/or KYA1797K. As the vehicle treatment, the treatment of BBR peptide alone did not affect the tumor growth and RAS degradation as shown by immunohistochemical (IHC) analyses and subsequent quantification (Fig EV5A–C). KYA1797K alone weakly suppressed the tumor growth, whereas the cotreatment of PTD-BBR and KYA1797K significantly reduced both the volume and weight of the tumors by 55 and 60%, respectively (Fig 6F). The cotreatments of PTD-BBR and KYA1797K, but not the treatment of KYA1797K alone, significantly reduced the levels of KRAS together with the ERK activities and PCNA levels, as well as the MT β-catenin-RAS interaction (Fig 6G). The RAS reduction and subsequent ERK inactivation by PTD-BBR and KYA1797K cotreatments were further confirmed by IHC analyses that showed reductions in p-ERK, the activity of its downstream transcription factor p-ATF2, and PCNA levels (Fig 6H). Overall, these data suggest that PTD-BBR restores the effects of KYA1797K on the inhibition of the synergistic growth of tumors that have both *CTNNB1* and *KRAS* mutations via the degradation of RAS, which was dissociated from MT β-catenin by PTD-BBR.

Discussion

The Wnt/β-catenin and RAS-ERK pathways are major signaling pathways for cellular transformation, and accumulating evidence indicates that both pathways synergistically interact in the tumorigenesis of CRC [5–7,19]. In particular, both *APC* and *KRAS* mutations, which occur in as many as 90 and 40–50% of CRC patients, respectively, critically accelerate the growth and transformation of CRC cells [7,19,20]. Moreover, both β-catenin and RAS proteins are highly increased in human CRC tissues not only via the initial stabilization of β-catenin by *APC* mutations but also via subsequent events that stabilize RAS, particularly the oncogenic mutant KRAS, which are the key events for signaling cross-talk involving the synergistic transformation [12]. However, the molecular details of the interaction of the two pathways in tumorigenesis are poorly understood.

In a resting status, RAS proteins are subjected to GSK3β-mediated phosphorylation at Thr-144 and Thr-148 residues, followed by the recruitment of the β-TrCP E3 linker, which leads to polyubiquitin-dependent proteasomal degradation [12,13]. Our previous observation that GSK3β-mediated RAS degradation is absent in CRC cells that express nondegradable MT β-catenin led us to identify a novel mechanism for the β-catenin-dependent sequential degradations of β-catenin and RAS via Wnt/β-catenin signaling. The stabilization of RAS in cells with accumulating β-catenin is attributed to the masking of the Thr-144 and Thr-148 phosphorylation sites by the binding of β-catenin at the α-interface, which can provide a large accessible surface area [18] as shown by NMR spectroscopy and *in vitro* pull-down analyses (Figs 2 and 3). Moreover, the exposure of these phosphorylation sites of RAS by prior β-catenin degradation enables access of GSK3β for phosphorylation and subsequent proteasomal degradation of RAS. However, the phosphorylation and degradation of RAS are dispensable for β-catenin degradation. These results indicate that β-catenin and RAS degradations by GSK3β-mediated phosphorylation occur in a stepwise manner. A prior β-catenin degradation, which subsequently exposes the Thr-144 and Thr-148 residues of RAS (I), is required for the GSK3β-mediated phosphorylation and subsequent polyubiquitination-dependent proteasomal degradation of RAS (II) (Fig 7, left panel). The accumulated β-catenin by its mutation masks the RAS phosphorylation sites and results in the costabilization of both proteins (Fig 7, right panel).

In summary, we have identified that a novel stepwise model for the degradation of both β-catenin and RAS and the costabilization of β-catenin and RAS, particularly the KRAS mutant form, by binding of the stabilized β-catenin due to its mutation or *APC* loss, play a critical role in the synergistic transformation of CRC cells. The role of the β-catenin-RAS interaction in the synergistic transformation and tumor growth induced by both *CTNNB1* and *KRAS* mutations has been further validated using a peptide blocking β-catenin-RAS interaction. This two-step model involving sequential degradations of β-catenin and RAS provides the pathological significance and a mechanical basis for the synergistic enhancement of colorectal tumorigenesis by genetic mutations of both pathway components. Moreover, in other types of cancer, such as gastric, breast, or liver cancers, in which *APC* mutations are not frequently identified, increments or aberrant activation of RAS, particularly mutant RAS, as well as β-catenin is observed [8,12,21–23]. Therefore, induction of the stepwise degradations of β-catenin and RAS by targeting the Wnt/β-catenin pathway may be an ideal approach for the treatment of various cancer types with aberrantly activated Wnt/β-catenin and RAS-ERK pathways attributed to the increment of β-catenin and RAS, particularly the mutant KRAS form, by *APC* loss or other reasons.

Materials and Methods

Cell lines

Human embryonic kidney (HEK) 293, HepG2 hepatocellular carcinoma, and DLD1 colorectal cancer (CRC) cells were purchased from the American Type Culture Collection (ATCC). Isogenic human CRC cells, HCT116 harboring WT or MT *CTNNB1* [24], were provided by B. Vogelstein (John Hopkins University School of Medicine, USA).
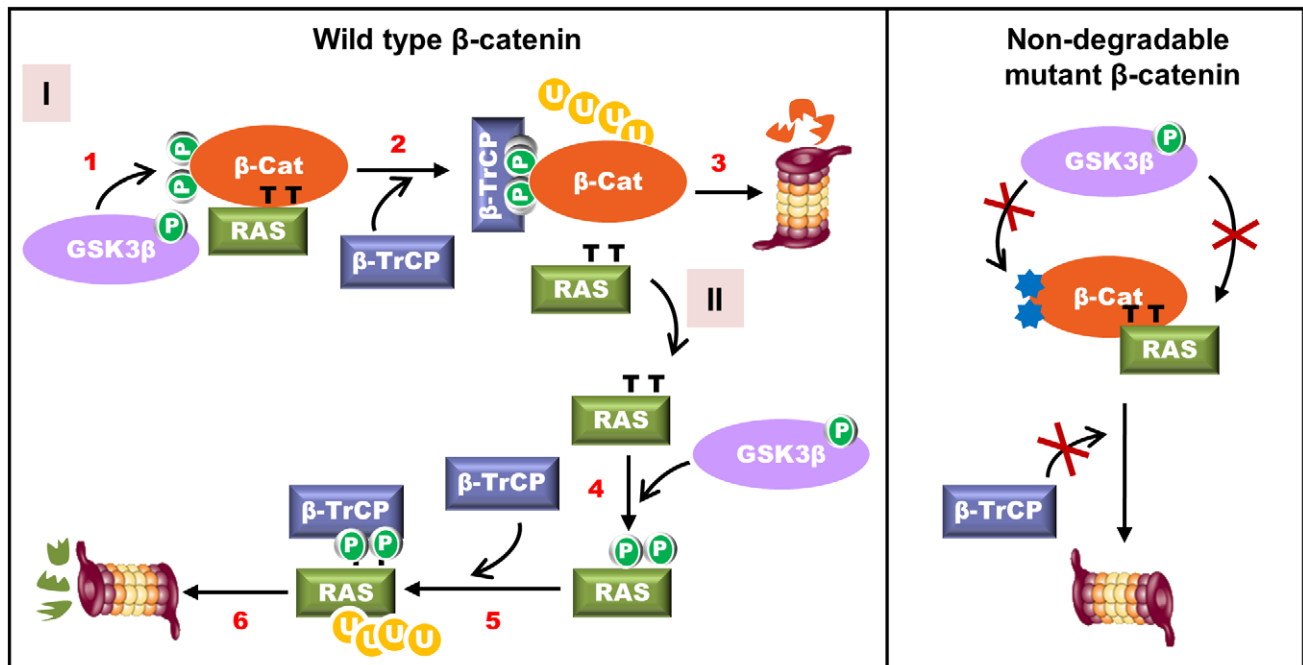
Figure 7. Schematic representation of stepwise models for β-catenin and RAS degradations depending on the *CTNNB1* mutation status.

Left panel: In a cell that expresses degradable WT β-catenin, the active GSK3β phosphorylates β-catenin at the Ser-33 and Ser-37 residues (number 1), followed by the recruitment of β-TrCP, which leads to polyubiquitination-dependent proteasomal degradation of β-catenin (numbers 2 and 3). As a second step (II), the released RAS by prior β-catenin degradation is subjected to phosphorylation by GSK3β at Thr-144 and Thr-148 (number 4), recruits β-TrCP (number 5), and is subsequently degraded through proteasome (number 6). Right panel: In a cell that expresses nondegradable MT β-catenin, RAS protein masked by MT β-catenin at the phosphorylation sites cannot be phosphorylated by GSK3β and costabilized with β-catenin. Blue stars represent mutation sites (Ser-33 and Ser-37) of β-catenin.

SW48 cells were provided by Won-Ki Kang (Division of Hematology-Oncology at Samsung Medical Center, Republic of Korea). HEK293, HepG2, and HCT116 were cultured in DMEM (Gibco BRL) supplemented with 10% fetal bovine serum (FBS; Gibco BRL). DLD1 and SW48 cells were maintained in RPMI 1640 (Gibco BRL) supplemented with 10% FBS.

Transfection and reagents

Lipofectamine (Invitrogen) and Lipofector-EZ (AptaBio) were used for plasmid or siRNA transfection, according to the manufacturer's instructions. Wnt3a-CM and L-CM were prepared as previously described [9]. All chemicals were dissolved in dimethyl sulfoxide (DMSO; Sigma-Aldrich) for the *in vitro* studies. When indicated, ALLN (25 µg/ml; Sigma-Aldrich) or MG132 (20 µM; Calbiochem) was added to the media to inhibit proteasomal protein degradation. The cells were treated with KYA1797K or XAV939 at a concentration of 5–20 µM for the indicated times. The two independent siRNA sequences for β-catenin were 5′-GAAACGGCTTTCAGTTGAG-3′ and 5′-AAACTACTGTGGACCACAAGC-3′ (Bioneer). The green fluorescence protein (GFP) siRNA used for the negative control was 5′-GUUCAGCGUGUCCGGCGAGTT-3′ (Bioneer).

Plasmids and constructs

The plasmids FLAG-WT-β-catenin-pcDNA3.0 and FLAG-S33Y-β-catenin-pcDNA3.0 were provided by Eric R. Fearon (University of Michigan, USA). The pCMV-WT-GSK3β-HA, pCMV-CA-GSK3β-HA (catalytic active form), and pCMV-KD-GSK3β-HA (catalytic inactive form) plasmids were provided by Jongkyeong Chung of Seoul National University (Republic of Korea). The Myc-WT-axin was provided by Eek-hoon Jho (University of Seoul, Republic of Korea). The pCS4-3xFlag-Ub was a gift from Dae-Won Kim (Yonsei University, Republic of Korea). The GFP-β-catenin-full-length (FL)-pEGFP-C1, GFP-β-catenin-ΔN86-pEGFP-C1, and GFP-β-catenin-ΔC110-pEGFP-C1 plasmids were provided by Kwonseop Kim (Chonnam National University, Republic of Korea). The constructs Myc-WT-NRAS-pcDNA3.1, Myc-WT-KRAS-pcDNA3.1, Myc-G12V-KRAS-pcDNA3.1, and Myc-G12V-KRAS-2A-pcDNA3.1 were previously generated [12,16]. The β-catenin binding region of KRAS (BBR) was amplified by the polymerase chain reaction (PCR) from the Myc-G12V-KRAS-pcDNA3.1 plasmid. The primers included 5′ *Bam*HI and 3′ *Xho*I restriction sites, which were used for the insertion of the products into the pEGX-4T-1 (Amersham) or pEGFP C1 (Clontech) vectors. His- or FLAG-tagged β-catenin constructs that contained FL, ΔN86, ΔC110, or C-terminal fragment (residues 661–782) were generated by PCR from the FLAG-WT-β-catenin-pcDNA3.0 plasmid. The PCR products of β-catenin deletion variants were subcloned into the 5′ *Bam*HI and 3′ *Sal*I-digested pET28a vector (EMD Biosciences). Mutagenesis of Thr-144 and Thr-148 to glutamic acid (T144/148E) on KRAS was performed with Myc-G12V-KRAS-pcDNA3.1 using the Quik-Change™ site-directed mutagenesis methods (Stratagene). PCR products were treated with the restriction endonuclease *Dpn*I

(Enzynomics) for 1 h and transformed into DH5α competent cells. The variant mutants of KRAS that contained ΔHVR, Δ131–165, and BBR-2E were generated by PCR-based mutagenesis. All constructs and mutations were confirmed by nucleotide sequencing analyses (Cosmogenetech).

Xenograft study

All animal experiments were performed in accordance with the Korean Food and Drug Administration guidelines. The protocols were reviewed and approved by the Institutional Animal Care and Use Committee (IACUC) of Yonsei University. The mice were housed in a microventilation cage system with a computerized environmental control system (Threeshine Inc.). The temperature was maintained at 24°C with a relative humidity of 45–55%. Athymic *nu/nu* mice were subcutaneously injected in the dorsal flank with MT HCT116 cells (1×10^7 cells/mice) in 200 μl of PBS: Matrigel® (1:1; BD Bioscience). When the mean tumor size reached 100–200 mm³, the mice were randomly divided into three groups: vehicle-, PTD-BBR-, KYA1797K-, or KYA1797K/PTD-BBR-treated groups. The tumor volumes were measured using vernier calipers every 4 day and were then calculated according to the following formula: π/6 × length × width × height. Twenty-eight days after drug treatment, the mice were sacrificed, and the tumors were excised and fixed in 4% paraformaldehyde (PFA) or snap-frozen in liquid nitrogen for further analyses.

Immunoblotting, immunoprecipitation, and ubiquitination assays

Cells were washed in ice-cold PBS and lysed using a radioimmunoprecipitation assay (RIPA) buffer that contained 10 mM of Tris (pH 7.4), 150 mM of NaCl, 1% NP-40, 0.1% deoxycholate, protease inhibitor cocktail (Sigma-Aldrich), 1 mM of PMSF, 2 mM of sodium fluoride, and 1 mM of sodium orthovanadate. Proteins were separated on 6–12% sodium dodecyl sulfate–polyacrylamide gel electrophoresis (SDS-PAGE) gels and transferred to a nitrocellulose membrane (Whatman). After blocking with 5% skim milk in Tris-buffered saline (TBS) for at least 1 h, the membranes were incubated with the indicated antibodies overnight, washed with TBS three times, and then incubated with horseradish peroxidase-conjugated secondary antibodies for 2 h. Immunoblotting was performed with the following antibodies: anti-pan-RAS monoclonal (clone RAS10, Millipore, MABS195; 1:2,000 and Santa Cruz Biotechnology, sc-4; 1:1,000), anti-β-catenin (Santa Cruz Biotechnology; sc-7199; 1:2,000), anti-p-β-catenin (S33/S37/T41; Cell Signaling Technology, #9561S; 1:1,000), anti-p-ERK (Cell Signaling Technology, #9101S; 1:4,000), anti-ERK (Santa Cruz Biotechnology, sc-514302; 1:5,000), anti-PCNA (Santa Cruz Biotechnology, sc-56; 1:1,000), anti-FLAG (Cell Signaling Technology, #2368; 1:4,000), anti-HA (Santa Cruz Biotechnology, sc-7392; 1:1,000), anti-K-RAS (Santa Cruz Biotechnology, sc-30; 1:1,000), anti-axin (Millipore Corporation, #06-022; 1:1,000), anti-β-TrCP (Cell Signaling Technology, #4394S; 1:2,000), anti-GSK3β (Cell Signaling Technology, #9315S; 1:2,000), anti-p-GSK3β (Y216; BD Bioscience, #612313; 1:1,000), anti-Myc (Santa Cruz Biotechnology, sc-40; 1:2,000), anti-GFP (Santa Cruz Biotechnology, sc-8334; 1:2,000), anti-GST (Santa Cruz Biotechnology, sc-374171; 1:5,000), and anti-α-tubulin (Cell Signaling Technology, #3873S; 1:5,000). The anti-p-

RAS antibody, which recognizes the phosphorylation of RAS proteins at Thr-144 and Thr-148, was described in our previous study [12]. Horseradish peroxidase-conjugated anti-mouse (Cell Signaling Technology, #7076; 1:4,000) or anti-rabbit (Bio-Rad; 1:4,000) secondary antibodies were used.

Immunoprecipitation and *in vivo* ubiquitination assays were performed as previously described [13]. Briefly, cells were washed in ice-cold PBS and lysed with RIPA buffer. For the *in vivo* ubiquitination assays, N-ethylmaleimide (NEM; Sigma-Aldrich; 10 mM) was subsequently added to the RIPA buffer. WCLs were incubated with the indicated antibodies and protein A/G agarose beads (Thermo Fisher Scientific) at 4°C for 12 h, and the beads were then washed three times with RIPA buffer. The resulting immune complexes were resolved by SDS–PAGE, and immunoblotting was performed with the indicated antibodies.

In vitro pull-down assays

To prepare the deletion variants of GST-HRAS and His-β-catenin fusion proteins, the *Escherichia coli* BL21 strain was transformed with pGEX4T-Mock, pGEX4T-HRAS (FL, ΔHVR, Δ131–165, and BBR), or pET-28a-β-catenin (FL, ΔN86, and ΔC110) plasmids and induced by 0.5 mM of isopropyl-1-thio-β-D-galactopyranoside (IPTG) for 4 h at 30°C. The cells were lysed in lysis buffer (1% Triton X-100 in PBS that contained a protease inhibitor cocktail) with sonication on ice. The purifications of these proteins from transformed bacterial cell extract have previously been described [12]. The purified soluble GST or His fusion proteins were immobilized on glutathione–agarose (Sigma-Aldrich) or Ni-NTA agarose (Invitrogen) beads and then mixed. The beads were washed with lysis buffer at least four times, and the pull-down samples were subsequently subjected to immunoblot analyses.

Fractionation experiment

MT HCT116 cells (2×10^7) were collected and resuspended in 500 μl of hypotonic lysis buffer (20 mM of HEPES (pH 7.4), 1.5 mM of MgCl₂, 10 mM of KCl, 0.25 M of sucrose, 1 mM of DTT, protease inhibitor, 1 mM of PMSF, and 1 mM of EDTA) for 10 min. After incubation, the cells were homogenized with a 25 G needle for 10 strokes and left on ice for 20 min. The sample was centrifuged at 2,000 × *g* at 4°C for 5 min. The nuclei pellet was washed with hypotonic buffer and then resuspended in 500 μl of nuclear extraction buffer (50 mM of Tris (pH 8.0), 120 mM of NaCl, 0.5% Nonidet P-40, 1 mM of DTT, protease inhibitor, 1 mM of PMSF, and 0.2 mM of EDTA) for 20 min on ice. The sample was centrifuged at 15,000 × *g* at 4°C for 20 min.

Immunocytochemistry

Cells were seeded on collagen-coated (500 μg/ml) coverslips and were treated or transfected with the indicated conditions. After incubation, the cells were fixed with 5% formalin for 30 min, permeabilized with 0.1% Triton X-100 for 20 min, and preblocked with PBS that contained 5% bovine serum albumin (BSA; Affymetrix) and 1% normal goat serum (NGS; Vector Laboratories) for at least 1 h. The cells were then incubated with the indicated primary antibody overnight at 4°C, followed by incubation with secondary antibodies

for 4 h at 4°C, and then counterstained with 4′, 6-diamidino-2-phenylindole (DAPI; Sigma-Aldrich) for 10 min at room temperature. After incubation, the cells were mounted in Gel/Mount media (Biomeda Corporation). The fluorescence signal was visualized using a confocal microscope (LSM510; Carl Zeiss) at excitation wavelengths of 488 nm (Alexa Fluor® 488), 543 nm (Alexa Fluor® 555), and 405 nm (DAPI).

In situ proximity ligation assay (PLA)

In situ PLA was performed using a Duolink II *In Situ* Red Starter Kit Mouse/Rabbit (Sigma-Aldrich) according to the manufacturer's manual. In brief, cells grown on collagen-coated (500 µg/ml) coverslips in 24-well plates were fixed, permeabilized, blocked, and incubated with anti-pan-RAS monoclonal (clone RAS10, Millipore, MABS195) and anti-β-catenin (Abcam; ab16051) antibodies at 4°C overnight. Duolink anti-rabbit PLUS and anti-mouse MINUS secondary antibodies and red detection reagents were used, and antibody incubation, ligation, amplification, and washing steps were performed according to the supplier's manual. Coverslips were then mounted using Duolink Mounting Media with DAPI and analyzed using a confocal microscope (LSM510; Carl Zeiss). The signal from the proximity ligation assay was quantified as the total red fluorescence signal divided by the DAPI signal to normalize the cellular content. In each experiment, 10 microscopic images that contained > 100 cells were quantified.

Cell proliferation and colony formation assays

For the cell proliferation assays, CRC cells were plated at a density of $2–5 \times 10^3$ cells/well in 96-well plates. The cells were then treated with the indicated conditions for 96 h. After incubation, 3-(4,5-dimethylthiazol-2-yl)-2-5-diphenyltetrazolium bromide (MTT; Amresco) reagent was added to each well at a concentration of 0.25 mg/ml for 2 h at 37°C, and insoluble purple formazan was subsequently obtained by removing the medium and extracting with DMSO. The absorbance at 590 nm was monitored with the FLUOstar Optima microplate reader (BMG Labtech). For the colony formation assays, CRC cells were seeded in 12-well plates (250–600 cells/well). The cells were treated with the indicated conditions for 7–16 days with changes in the medium every 4 days. At the end of the experiment, cells were washed and fixed/stained with 0.5% crystal violet in 20% ethanol for 2 h and then washed three times with distilled water.

Protein expression and purification for nuclear magnetic resonance (NMR) spectroscopy and fluorescence analyses

Human β-catenin (FL and C-terminal region, residues 661–781) and KRAS-G12V (FL and BBR, residues 110–165), which were amplified by PCR from intact FLAG-β-catenin-pcDNA3.1 and Myc-KRAS-G12V-pcDNA3.1, were inserted into the pET21b vector (Novagen) with the N-terminal hexa-histidine tag and *Tobacco etch* virus (TEV) protease cleavage site (ENLYFQG). These recombinant plasmids were transformed into *E. coli* BL21 (DE3). Bacterial cells were grown in LB media with ampicillin (100 µg/ml) at 37°C until the optical density at 600 nm reached approximately 0.6, at which time IPTG was added to a concentration of 0.2 or 1 mM, and the cells

were incubated for an additional 20 h at 18°C. To prepare uniformly ^{15}N- and ^{13}C/^{15}N-labeled proteins for the NMR spectroscopy experiments, the cells were cultured in M9 media that contained ^{15}NH$_4$Cl (Cambridge Isotope Lab) as the source of nitrogen and ^{13}C-D-glucose. The cell pellets were lysed by sonication in lysis buffer that contained protease inhibitor cocktail (for KRAS-FL, 40 mM of HEPES, 300 mM of NaCl, 5 mM of MgCl$_2$, 5 mM of β-mercaptoethanol, pH 8.0; for KRAS-110-165, 25 mM of NaPi, 300 mM of NaCl, 10 mM of BME, pH 6.8; for β-catenin-FL, 20 mM of NaPi, 50 mM of NaCl, 10 mM of β-mercaptoethanol, pH 8.0 with 10% glycerol, 0.1% Triton X-100; for β-catenin-661-781, 25 mM of HEPES, 300 mM of NaCl, pH 7.5). His- or Trx-His-tagged fusion proteins were purified by immobilized metal affinity chromatography using Ni-NTA columns (Amersham Pharmacia). The proteins were cleaved by TEV protease treatment at 25 or 4°C. These proteins were then purified by Ni-NTA columns and size exclusion chromatography.

Fluorescence spectroscopy

The binding constants between KRAS and β-catenin were measured by a LS55 fluorescence spectrophotometer (PerkinElmer). β-Catenin protein in buffer that contained 20 mM of NaPi, 50 mM of NaCl, and 10 mM of β-mercaptoethanol, pH 8.0, was titrated with KRAS to a molar ratio of 1:0 to 1:0.6 using a thermostat cuvette. The values detected at the same concentration of ligand only were subtracted for the calibration of the inherent intensities of the protein ligands. The dissociation constant (K_d) values were calculated using the following equation: $\log (F_0\text{-}F/F) = \log (1/K_d) + n \log [\text{ligand}]$, where F_0 and F represent the fluorescence intensities of the protein at 343 nm in the absence and presence of ligand, respectively, and the number n represent the ligand binding sites of the protein [25].

NMR spectroscopy titration

All NMR experiments were performed at 298K on a Bruker Avance 600 MHz instrument (Billerica), and 2D ^{1}H-^{15}N HSQC experiments were performed with the following conditions: 90% H$_2$O/10% ^{2}H$_2$O NMR buffer that contained 50 mM of HEPES, 50 mM of NaCl, 2 mM of MgCl$_2$, 2 mM of dithiothreitol (DTT), pH 7.4. For NMR titration experiments, ^{15}N-labeled KRAS was purified from M9 media that contained ^{15}NH$_4$Cl, and β-catenin was obtained from LB media. The ^{1}H-^{15}N HSQC spectra were obtained at various molar ratios of ^{15}N-labeled proteins with respect to partner proteins. The concentration of ^{15}N-labeled KRAS was 0.2 mM, and the molar ratios of ^{15}N-labeled KRAS and β-catenin were 1:1, 1:5, and 1:10. All collected spectra were processed and analyzed using nmrPipe/nmrDraw (Biosym/Molecular Simulation) software [26] and the PINE-SPARKY program [27]. Sequential resonance assignments were used as previously reported (Biological Magnetic Resonance Bank 18529) [28]. The KRAS structure with the PDB code 2MSC [18] was used to determine the binding modes of KRAS and β-catenin.

PTD-BBR peptide synthesis and analyses

To prepare the BBR peptide for *in vivo* xenograft experiments, a C-terminus FITC-conjugated protein transduction domain (PTD)-β-catenin binding region of KRAS (BBR; residues 139–153) peptide

was designed and synthesized with the following sequence (Peptide 2.0): RRRRRRRR (PTD)-GGGG (linker)-PFIETSAKTRQGVDK (BBR)-FITC. For the analysis of the transduction ability of PTD-BBR, MT HCT116 cells were treated with 1–20 μM of PTD-BBR for 24 h and were subsequently analyzed by flow cytometry (Accuri™ Cytometer; BD Bioscience) and immunocytochemistry.

Immunohistochemistry (IHC)

For the IHC analyses, the sections were incubated overnight at 4°C with the indicated primary antibody. The sections were subsequently incubated with anti-mouse Alexa Fluor® 488 (Life Technologies, A11008; 1:500) or anti-rabbit Alex Fluor® 555 (Life Technologies, A21428; 1:500) secondary antibodies for 1 h at room temperature. The sections were then counterstained with DAPI and mounted in Gel/Mount media. All incubations were conducted in dark, humid chambers. The fluorescence signal was visualized using a confocal microscope (LSM510; Carl Zeiss) at excitation wavelengths of 488 nm (Alexa Fluor® 488), 543 nm (Alexa Fluor® 555), and 405 nm (DAPI). At least three fields per section were analyzed.

Cell cycle and apoptosis assays

HCT116 cells were treated with 10 μM of PTD-BBR and/or 20 μM of KYA1797K for 24 h. For the analysis of the cell cycle, cells were fixed with 70% ethanol for 1 h and stained with 50 μg/ml of propidium iodide (PI; Sigma-Aldrich) that contained 100 μg/ml of RNase (Sigma-Aldrich) for 30 min. The cell cycle profile was analyzed by BD FACSCalibur (BD Biosciences). For the apoptosis assay, cells were harvested and then resuspended in binding buffer (10 mM of HEPES, 140 mM of NaCl, and 2.5 mM of $CaCl_2$) at a concentration of 1×10^6 cells/ml. One hundred microliters of the cell suspension was incubated with 5 μl of APC Annexin V (Biolegend) and 2 μl of PI for 15 min in the dark. Four hundred microliters of binding buffer was added to each tube, and the cells were analyzed using an SA3800 spectral analyzer (Sony Corporation). The quadrant lines for each sample were adjusted using unstained, Annexin V-stained, and PI-stained cells as a control.

Quantification and statistical analysis

All data are represented as the mean ± standard deviation (SD), and the number of samples was indicated in each figure legend. The statistical significance of the differences was assessed using the two-sided Student's *t*-test. The results shown are representative of at least three independent experiments. Significance was denoted as *$P < 0.05$, **$P < 0.01$, and ***$P < 0.001$.

Expanded View for this article is available online.

Author contributions

S-KL, W-JJ, Y-HC, P-HC, J-SY, and EJR designed and performed all experiments. SHC, J-MO, YSH, and WTL performed the fluorescence spectroscopy analysis, NMR spectra, and structural analysis. HTK and GHH synthesized chemicals. S-KL, W-JJ, Y-HC, P-HC, EJR, DSM, and K-YC performed the data analysis and wrote the manuscript. All authors reviewed and edited the manuscript.

Conflict of interest

The authors declare that they have no conflict of interest.

References

1. Fodde R (2002) The APC gene in colorectal cancer. *Eur J Cancer* 38: 867–871
2. Polakis P (1999) The oncogenic activation of beta-catenin. *Curr Opin Genet Dev* 9: 15–21
3. Downward J (2003) Targeting RAS signalling pathways in cancer therapy. *Nat Rev Cancer* 3: 11–22
4. Kinzler KW, Vogelstein B (1996) Lessons from hereditary colorectal cancer. *Cell* 87: 159–170
5. D'Abaco GM, Whitehead RH, Burgess AW (1996) Synergy between Apc min and an activated ras mutation is sufficient to induce colon carcinomas. *Mol Cell Biol* 16: 884–891
6. Horst D, Chen J, Morikawa T, Ogino S, Kirchner T, Shivdasani RA (2012) Differential WNT activity in colorectal cancer confers limited tumorigenic potential and is regulated by MAPK signaling. *Cancer Res* 72: 1547–1556
7. Sansom OJ, Meniel V, Wilkins JA, Cole AM, Oien KA, Marsh V, Jamieson TJ, Guerra C, Ashton GH, Barbacid M *et al* (2006) Loss of Apc allows phenotypic manifestation of the transforming properties of an endogenous K-ras oncogene *in vivo*. *Proc Natl Acad Sci USA* 103: 14122–14127
8. Zeller E, Hammer K, Kirschnick M, Braeuning A (2013) Mechanisms of RAS/β-catenin interactions. *Arch Toxicol* 87: 611–632
9. Yun M-S, Kim S-E, Jeon SH, Lee J-S, Choi K-Y (2005) Both ERK and Wnt/beta-catenin pathways are involved in Wnt3a-induced proliferation. *J Cell Sci* 118: 313–322
10. Park K-S, Jeon SH, Kim S-E, Bahk Y-Y, Holmen SL, Williams BO, Chung K-C, Surh Y-J, Choi K-Y (2006) APC inhibits ERK pathway activation and cellular proliferation induced by RAS. *J Cell Sci* 119: 819–827
11. Jeon SH, Yoon JY, Park YN, Jeong WJ, Kim S, Jho EH, Surh YJ, Choi KY (2007) Axin inhibits extracellular signal-regulated kinase pathway by Ras degradation via beta-catenin. *J Biol Chem* 282: 14482–14492
12. Jeong WJ, Yoon J, Park JC, Lee SH, Kaduwal S, Kim H, Yoon JB, Choi KY (2012) Ras stabilization through aberrant activation of Wnt/beta-catenin signaling promotes intestinal tumorigenesis. *Sci Signal* 5: ra30
13. Kim SE, Yoon JY, Jeong WJ, Jeon SH, Park Y, Yoon JB, Park YN, Kim H, Choi KY (2009) H-Ras is degraded by Wnt/beta-catenin signaling via beta-TrCP-mediated polyubiquitylation. *J Cell Sci* 122: 842–848
14. Moon B-S, Jeong W-J, Park J, Kim TI, Min DS, Choi K-Y (2014) Role of oncogenic K-Ras in cancer stem cell activation by aberrant Wnt/β-catenin signaling. *J Natl Cancer Inst* 106: djt373
15. Cho YH, Cha PH, Kaduwal S, Park JC, Lee SK, Yoon JS, Shin W, Kim H, Ro EJ, Koo KH *et al* (2016) KY1022, a small molecule destabilizing Ras via targeting the Wnt/beta-catenin pathway, inhibits development of metastatic colorectal cancer. *Oncotarget* 7: 81727–81740
16. Cha PH, Cho YH, Lee SK, Lee J, Jeong WJ, Moon BS, Yun JH, Yang JS, Choi S, Yoon J *et al* (2016) Small-molecule binding of the axin RGS domain promotes beta-catenin and Ras degradation. *Nat Chem Biol* 12: 593–600

17. Liu C, Li Y, Semenov M, Han C, Baeg GH, Tan Y, Zhang Z, Lin X, He X (2002) Control of beta-catenin phosphorylation/degradation by a dual-kinase mechanism. *Cell* 108: 837−847

18. Mazhab-Jafari MT, Marshall CB, Smith MJ, Gasmi-Seabrook GM, Stathopulos PB, Inagaki F, Kay LE, Neel BG, Ikura M (2015) Oncogenic and RASopathy-associated K-RAS mutations relieve membrane-dependent occlusion of the effector-binding site. *Proc Natl Acad Sci USA* 112: 6625−6630

19. Janssen KP, Alberici P, Fsihi H, Gaspar C, Breukel C, Franken P, Rosty C, Abal M, El Marjou F, Smits R *et al* (2006) APC and oncogenic KRAS are synergistic in enhancing Wnt signaling in intestinal tumor formation and progression. *Gastroenterology* 131: 1096−1109

20. Fearon ER, Vogelstein B (1990) A genetic model for colorectal tumorigenesis. *Cell* 61: 759−767

21. Network CGAR (2014) Comprehensive molecular characterization of gastric adenocarcinoma. *Nature* 513: 202−209

22. Carey L, Winer E, Viale G, Cameron D, Gianni L (2010) Triple-negative breast cancer: disease entity or title of convenience? *Nat Rev Clin Oncol* 7: 683−692

23. Vilchez V, Turcios L, Marti F, Gedaly R (2016) Targeting Wnt/β-catenin pathway in hepatocellular carcinoma treatment. *World J Gastroenterol* 22: 823

24. Chan TA, Wang Z, Dang LH, Vogelstein B, Kinzler KW (2002) Targeted inactivation of CTNNB1 reveals unexpected effects of β-catenin mutation. *Proc Natl Acad Sci USA* 99: 8265−8270

25. Jiang Y, Fang X, Bai C (2004) Signaling aptamer/protein binding by a molecular light switch complex. *Anal Chem* 76: 5230−5235

26. Delaglio F, Grzesiek S, Vuister GW, Zhu G, Pfeifer J, Bax A (1995) NMRPipe: a multidimensional spectral processing system based on UNIX pipes. *J Biomol NMR* 6: 277−293

27. Lee W, Westler WM, Bahrami A, Eghbalnia HR, Markley JL (2009) PINE-SPARKY: graphical interface for evaluating automated probabilistic peak assignments in protein NMR spectroscopy. *Bioinformatics* 25: 2085−2087

28. Vo U, Embrey KJ, Breeze AL, Golovanov AP (2013) (1)H, (1)(3)C and (1)(5)N resonance assignment for the human K-Ras at physiological pH. *Biomol NMR Assign* 7: 215−219